Petroleum Science 21 (2024) 1474–1487

Contents lists available at ScienceDirect

Petroleum Science

journal homepage: www.keaipublishing.com/en/journals/petroleum-science

Original Paper

Concise extraction and characterization of the pore-throat network in unconventional hydrocarbon reservoirs: A new perspective

Shu-Heng Du [a, b, c, *], Yong-Min Shi [c]

[a] State Key Laboratory of Nonlinear Mechanics, Institute of Mechanics, Chinese Academy of Sciences, Beijing, 100190, China
[b] School of Engineering Science, University of Chinese Academy of Sciences, Beijing, 100049, China
[c] School of Earth and Space Sciences, Peking University, Beijing, 100871, China

ARTICLE INFO

Article history:
Received 19 April 2023
Received in revised form
25 July 2023
Accepted 11 December 2023
Available online 22 December 2023

Edited by Jie Hao and Meng-Jiao Zhou

Keywords:
Hydrocarbon exploitation
Pore
Throat
Porous media
Identification

ABSTRACT

In this study, a new image-based method for the extraction and characterization of pore-throat network for unconventional hydrocarbon storage and exploitation is proposed. “Pore-throat solidity”, which is analogous to particle solidity, and a new method for automatic identification of pores and throats in tight sandstone oil reservoirs are introduced. Additionally, the “pore-throat combination” and “pure pore” are defined and distinguished by drawing the cumulative probability curve of the pore-throat solidity and by selecting an appropriate cutoff point. When the discrete grid set is recognized as a pore-throat combination, Legendre ellipse fitting and minimum Feret diameter are used. When the pore and throat grid sets are identified as pure pores, the pore diameter can be directly calculated. Using the new method, the analytical results for the physical parameters and pore radius agree well with most prior studies. The results comparing the maximum ball and the new model could also prove the accuracy of the latter's in micro and nano scales. The new model provides a more practical theoretical basis and a new calculation method for the rapid and accurate evaluation of the complex processes of oil migration.

1. Introduction

Unconventional reservoirs have become the new main focus of energy exploration and development (Jia et al., 2014; Zou et al., 2015). Similar to conventional reservoirs, unconventional reservoir still depend on the development of reservoir spaces, which can be divided into three types: holes, fractures, and pores. Holes are mainly distributed in carbonate rocks; fractures and pores are mainly distributed in clastic rocks (Sheng et al., 2020; Jin et al., 2022). The pore system can be further subdivided into pores and throats (Luo et al., 2022; Bai et al., 2014; Lai et al., 2018b). The space surrounded by rock particles and not filled by cement and miscellaneous foundation is defined as pore; the relatively narrow space between particles is defined as throat (Zhang et al., 2021; Luo et al., 2022). The formation of pores and throats is due to the accumulation, compaction, and subsequent diagenesis of mineral particles (Wang et al., 2022; Yang et al., 2022). They are formed by the primary and secondary boundaries of particles (i.e., for pores and throats, the grain boundaries after denudation, transportation, and reconstruction). Furthermore, the pore and throat characteristics largely reflect the sorting and roundness of particles, which is a reflection of the results of deposition, compaction, and modification (Visher, 1969; Cao et al., 2021; Jiu et al., 2021). Therefore, an obvious symbiotic relationship exists between the formation of pores and throats and the formation of particles during deposition (Yang et al., 2021; Liu et al., 2022).

Pores and throats are closely connected in the reservoir. Generally, pores determine reservoir capacity, and throats determine productivity. In order to evaluate the reservoir capacity and productivity respectively from the perspective of reservoir characterization, it is necessary to find the key differences in physical properties between pores and throats and then put forward corresponding theoretical and experimental methods to distinguish pores and throats. The physical property distribution of pores and throats can be obtained, respectively, and the impact mechanism on reservoir and seepage can also be investigated. Above descriptions are the definition and the necessity of “pore throat identification” (Cai et al., 2019; Wang et al., 2019; Kong et al., 2020; Zhang et al., 2020, 2021).

* Corresponding author.
E-mail address: dushuheng@imech.ac.cn (S.-H. Du).

https://doi.org/10.1016/j.petsci.2023.12.009

1.1. Pore and throat identification based on image processing

Nowadays, the identification method of pore and throat mainly depends on image processing technology (Li et al., 2021a; Wood, 2021; Liu et al., 2022). With the help of advanced imaging technologies such as electron microscope and computed tomography (CT), researchers can observe the reservoir space and obtain images with different resolutions directly (Lyu et al., 2021b). In order to achieve the purpose of pore and throat identification, researchers mainly focus on how to accurately describe the morphological differences between pore and throat based on image processing technology (Li et al., 2021a, 2021b; Liu et al., 2022). The maximum ball (MB) method to address the scanning data of CT are proposed to obtain the quantitative distribution of pores and throats. All the largest balls are generated in the reservoir space, the spherical wall is tangent to the inner boundary of the reservoir space and does not belong to each other. It is the basic unit used to characterize the connectivity of pore geometry. The set of all the largest balls defines all the storage spaces together (Silin et al., 2003; Dong, 2008). In the theoretical model of MB, the maximum or minimum radius of an inner tangential circle are treated as the approximate pore or throat size (Yin et al., 2021a; Xie et al., 2022). In order to improve the accuracy of pore and throat identification and simplify the calculation program furtherly, researchers have proposed a series of new methods for pore and throat identification based on different algorithms, including the city block distance function and watershed identification algorithm (Rabbani et al., 2014), the method of pore reconstruction and partitioning (Van Eyndhoven et al., 2015), the implementation of pore structure model generation and pore space analysis tools (Putanowiczet al., 2015), the method based on fractal dimension analysis (Liu et al., 2015; Lai et al., 2016; Lai and Wang, 2015; Lai et al., 2018a; Xiong et al., 2017), the updated MB method (Liu et al., 2012; Gong et al., 2016; Arand and Hesser, 2017), the deformation function method based on synchrotron X-ray microphotography (Arzilli et al., 2016; Smal et al., 2018), the method based on SEM image (Gundogar et al., 2016), the nonlinear programing and optimization techniques (Sharqawy, 2016), the new pore network extraction (PNE) model (Zhou et al., 2017) and the automatic image processing method based on thin-walled lithofacial microscopy (Van Eyndhoven et al., 2015; Berrezueta and Kovacs, 2017). Through the above series of methods, the pore-throat type, pore geometry, pore size, pore connectivity can be calculated, which could provide important insights into the microscopic pore structure characteristics of tight sandstones. But frankly, most of the above pore and throat identification methods only focus on the morphological differences between pore and throat, the influence of flow factors on pores and throats is not frequently considered, and it is unclear if this will lead to a lack of physical significance for pore size because the research on pore-throat identification and characterization is aimed at clarifying the flow law of oil, gas, and water. As to the above identification methods, the higher the resolution requirements, the smaller the sample size (usually less than 2 mm). Thus, the representativeness and applicability are greatly reduced in a reservoir that display high heterogeneity (Gundogar et al., 2016; Sharqawy, 2016; Arand and Hesser, 2017; Smal et al., 2018).

1.2. Pore and throat identification based on fluid injection

In addition to image processing, researchers also use the fluid injection experiment to realize the identification of pore and throat. Based on the Young-Laplace equation describing the relationship between capillary radius and capillary pressure, and with the help of constant-rate mercury injection, researchers can obtain the distribution of pores and throats indirectly.

During the experimental process of constant-rate mercury injection, mercury is injected at a low rate (0.001 μL/s), ensuring the occurrence of quasi-static process. In this process, the interfacial tension and contact angle remain unchanged; each pore shape change experienced by the mercury inlet front will change the shape of the meniscus, resulting in the change of the capillary pressure of the system. The rise of capillary pressure indicates the throat, and the fall of capillary pressure represents the pore. Therefore, researchers can distinguish the throat and pore of sandstone, carbonate rock, shale and other reservoirs, describe the development characteristics of throat and pore, respectively.

Obviously, due to the pressure limit of the experimental instrument (6.2 MPa), some pores and throats with small radius will be omitted in the process of the experiment, so this type of technology can not reflect the complete distribution of pores and throats which needs to be investigate furtherly (Jiang et al., 2021; Yin et al., 2021b).

1.3. Comparison of existing research methods

It can be clearly seen that the existing research methods have their own advantages and disadvantages. The high-pressure mercury injection test obtains the apparent throat radius, which cannot reflect the pores. Although constant-rate mercury injection can distinguish pores and throats, many small-scale pores and throats in tight sandstone are ignored due to its low pressure. Nuclear magnetic resonance can identify most of the reservoir spaces, but cannot distinguish pores from throats. Moreover, above techniques cannot observe pores and throats directly. Although CT technology can achieve high resolution, it is difficult to balance resolution and observation size, which will affect the reliability of conclusions.

Despite the advances from the aforementioned studies, at least four major unsolved problems still remain. First, for a reservoir sample, the matching degree of pore and throat information obtained by theoretical and experimental methods is poor. Second, the comparability of results obtained by different techniques is poor due to the principles of the various quantitative techniques, which causes some difficulty in application. Third, currently image analysis mainly relies on visual observations and manual measurement, instead of automatic identification and statistical analysis. Fourth, the accurate quantitative identification criteria for pores and throats of tight sandstone oil reservoirs in two-dimensional (2D) space is still lacking. Therefore, it is necessary to propose a new model for pore and throat identification. The proposed model should not only reflect the morphological differences of pores and throats quantitatively, but also show the physical properties of pores and throats as flow space clearly. In addition, the model also needs to take into account the resolution and sample size. Actually, the above new identification model is the ultimate goal of this paper.

2. Research background

The Ordos Basin, located in the western part of the North China Block, is a large-scaled multicycle cratonic basin with the characteristics of simple structure and integrated uplifts as well as subsidence and depression migration (Darby and Ritts, 2002). Based on tectonic development, sedimentary patterns, and structure of Ordovician strata, the Paleozoic sequence of the Ordos Basin is represented by six tectonic units: the Western Edge Fold Belt, Tianhuan Depression, Shanbei Slope, Jinxi Fault and Fold Belt, Weibei Uplift, and Yimeng Uplift (Gan et al., 2007; Wang et al., 2015).

In terms of stratigraphy and depositional facies, the Triassic Yanchang Formation, the basin's main hydrocarbon reservoir, is

characterized by its large areas, with lake delta front and delta plain deposits. The correlation between the basin's physical properties and its ability to yield oil is strong. The distribution range of sand bodies controls the distribution range of reservoirs, which is conducive to the formation of large-scale stratigraphic trap (Du et al., 2018a). Sandstone and mudstone boundaries are generally flat and extensive. Furthermore, it is easy to distinguish a single sand body with a thickness of about 3 m. Finally, the phenomenon of a sand body pinch out is evident in some places, and the interlayer is widely developed (Du et al., 2018b).

The location of the study area is shown in Fig. 1 (Du et al., 2019). It is located in the southwestern part of the northern Shanbei Slope in the Ordos Basin.

The Chang 7 members of the Yanchang Formation are dominated by clastic lacustrine sediments from the late Triassic period. The physical properties are poor: the average porosity is 8.85%, and the permeability is 0.16×10^{-3} μm^2. The pore types are mainly inter-granular or dissolved, and the primary inter-granular pores, secondary inter-granular pores, and secondary dissolved pores. (Li et al., 2011; Du et al., 2018a; 2018b).

Having conducted a comprehensive survey of the study area, we determined that the Chang 7_2 member (as opposed to Chang 7_1 and Chang 7_3) of the Yanchang Formation is the main oil producing layer (Liu et al., 2021; Xu et al., 2021).

Three typical sedimentary cycles occur in the Chang 7_2 member. Fig. 2 shows the typical sedimentary characteristics of an underwater distributary channel. The position of the channel swings frequently, which impacts microscopic heterogeneity of the Chang 7_2 reservoir. The lithology of the tight sandstone reservoir in the study area is mainly gray-white medium-fine feldspathic sandstone, including lithic feldspathic sandstone and feldspathic lithic sandstone, with its compositional maturity (Guo et al., 2012; Yang and Deng, 2013). Moreover, the micro-interlaced bedding and wedge-shaped interlaced bedding are well developed in the reservoirs. Common scouring surfaces reflect strong hydrodynamic conditions and represent the typical characteristics of the microfacies of underwater distributary channel sedimentation (Liu et al., 2015; Yao et al., 2018).

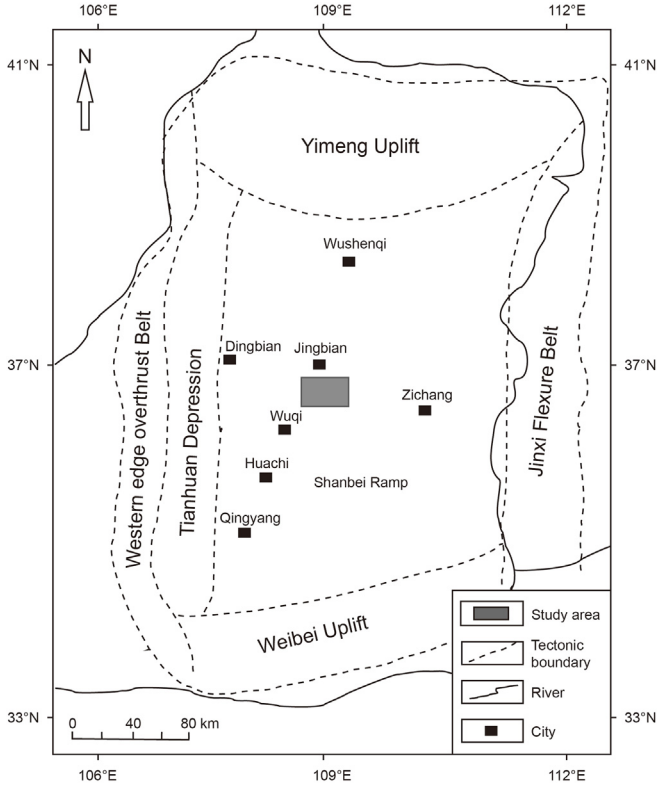

Fig. 1. Study area location in the Ordos Basin, China. (Note: The gray square indicates the location of the Yanchang Formation core.)

3. Principles and methods

3.1. Proposal of the concept of pore-throat solidity

To clarify and characterize the influence of pores and throats in tight sandstone oil reservoirs, pore-throat identification should be performed. Microscopy and a simplified model are used to describe the feature differences between pores and throats. In this paper, from the perspective of morphology, we examine pores and throats, finding new identification criteria. Using reservoir images, two types were identified: the “pore-throat combination” and the “pure pore.”

Russ (1998) and Faria et al. (2003) proposed the concept of particle solidity for the shape of particles, using the following Eq. (1):

$$S = \frac{S_p}{S_c} \tag{1}$$

where S, S_p and S_c represent particle solidity, particle area, the area of the particle boundary's convex hull, respectively.

Analogous to particle solidity, the concept of “pore-throat solidity” is introduced in this paper (Fig. 3), which was used to characterize the concave and convex degrees of pores and throats (Zeng et al., 2020):

$$S' = \frac{S'_p}{S'_c} \tag{2}$$

where S', S'_p and S'_c represent pore-throat solidity, pore-throat area, the area of the pore-throat boundary's convex hull, respectively.

As evident in Fig. 3, the calculation process for “S'_p” and “S'_c” was obtained. “a” can be calculated as the total area of the pixel points occupied in a pore or throat; “b” can be calculated as the total of the pixel points occupied in the convex hull area, which covers all of area “S'_p”.

In this study, pure pores contain only the discrete grids of pores from the perspective of morphology; the pure pore has decisive significance for the accumulation of oil and gas, but it has no obvious significance for the fluid flow process (Fig. 4(a)–(c)). The pore-throat combination contains the grids of both pores and throats (the latter being the relatively narrow part between two pores), which has significance for the fluid flowing process (Fig. 4(d)–(f)).

As a result of the process of particulate transport, sorting, roundness, and accumulation, Visher (1969) distinguished the transport mode of particles (e.g., rolling, jumping, and levitation) by the inflection point in the cumulative particle size probability distribution curve. Similarly, based on the symbiotic relationship between pores, throats, and particles, we can select the appropriate parameters of the pore morphology and draw the cumulative probability curve by selecting the appropriate cutoff point to distinguish the pore-throat combination and the pure pore.

3.2. Computing principles of pore-throat solidity

To apply innovative ideas and methods through a software program, a corresponding mathematical theory and reasonable

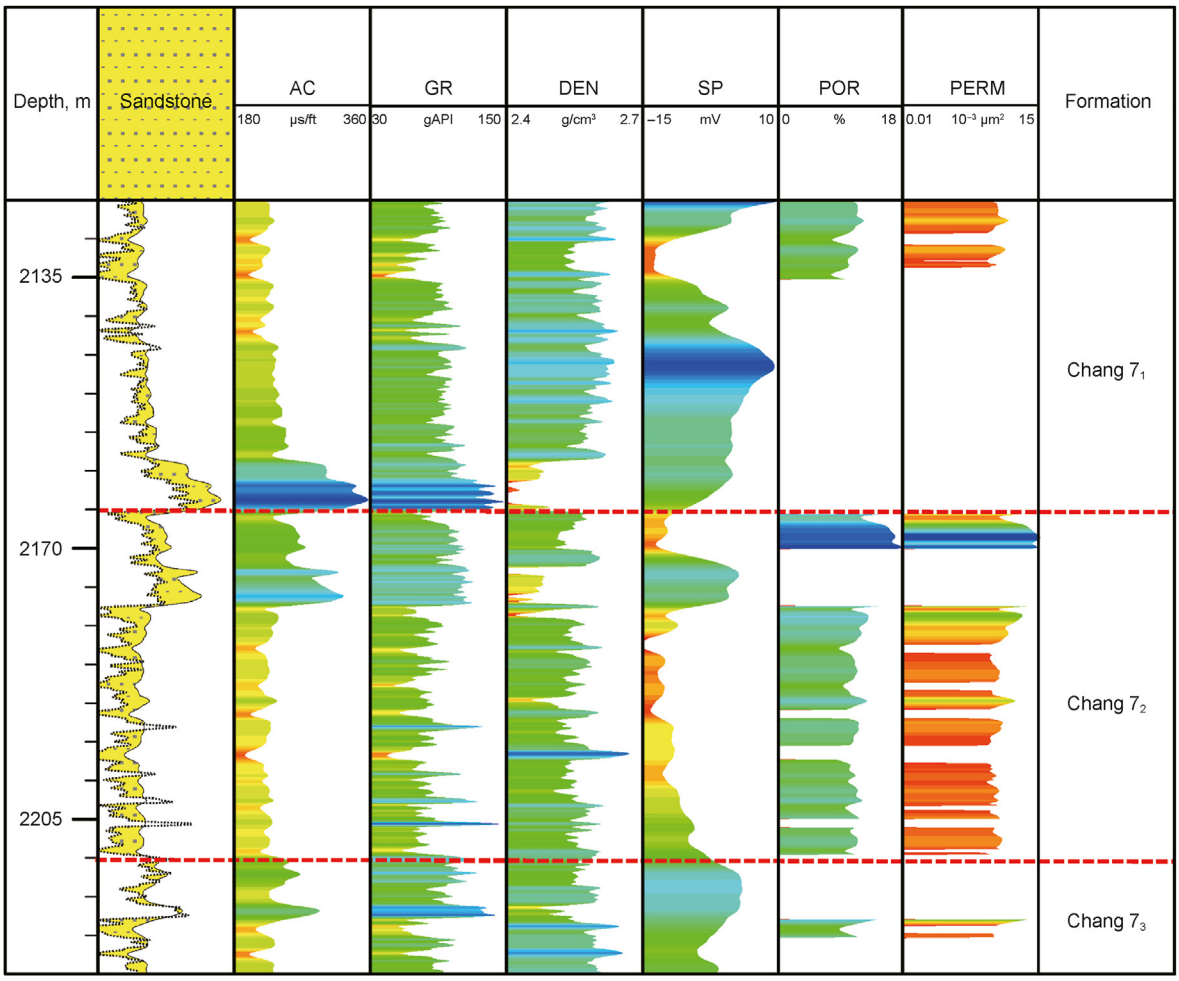

Fig. 2. Composite log curves of the Chang 7 members' tight sandstone oil reservoir in the Yanchang Formation, Well A83, Ordos Basin. (Note: AC = acoustics, us/ft, GR = natural gamma rays, gAPI, DEN = density, g/cm^3, SP = spontaneous potential, mV, POR = porosity, %, and PERM = permeability, 10^{-3} μm^2. The two red dotted lines indicate the interfaces of the three parts of the Chang 7 members of the Yanchang Formation: Chang 7_1, Chang 7_2, and Chang 7_3. The yellow parts in the second column indicate the sandstone reservoir in which the relative areas could reflect reservoir quality.).

program should be introduced to conduct Legendre ellipse fitting and the minimum Feret diameter calculation for pore-throat solidity.

First, Jarvis March and the gift wrapping algorithm in computational geometry is introduced (Jarvis, 1973; Cormen et al., 2001). The pore-throat solidity parameters are constructed based on the description of pore and throat shapes. The process is as followings (see also Fig. 3(b)): (1) select the extracted pore-throat grid set S as the target point set; (2) start from $i = 0$, where the first point is P_0 (the leftmost point) on the convex hull; (3) select the point P_{i+1} to ensure that all points are on the right side of the online P_iP_{i+1}; (4) make $i = i + 1$ and repeat until $P_h = P_0$, reaching the convex hull again. The entire program is similar to the process of wrapping a string around grouped points.

Second, the theory of the Legendre inertia ellipse in geometric analysis is introduced (Mikli et al., 2001; Pirard, 2004). Legendre inertia ellipse fitting of pores and throats is conducted (Fig. 5), and the centroid of elliptic pores and throats is located in the center of the Legendre inertia ellipse. It has the same geometric moments with the original area of the essential pore and throat. In Fig. 3, the "a" area, the long- and short-axis lengths are both the robust parameters.

Third, the theory of the Feret diameter for computational physics was introduced (Walton, 1948; Faria et al., 2003). When pores and throats are chosen as research objects, the Feret diameter is used to measure the distance between parallel lines of the pore and throat boundaries along a given direction. The shortest distance is the minimum Feret diameter (i.e., the width of the pore and throat), and this diameter is calculated for the identified pores and throats. Moreover, to ensure accuracy, at least three sections of pores and throats must be obtained, cutting from different directions. The distribution of the pores and throats separately must then be calculated so that the average of the multidirectional data can reflect the pore and throat distribution more precisely.

When the discrete grid set is recognized as the pore-throat combination, Legendre ellipse fitting and the minimum Feret diameter are used. Since the Legendre elliptical axis length and the minimum Feret diameter are both robust parameters characterizing the width of the pore and throat (Faria et al., 2003), the minimum width of the Legendre ellipse length and the minimum Feret diameter can be calculated to accurately quantify throat width (Fig. 5).

When the pore and throat grid sets are identified as pure pores, the pore diameter can be directly calculated.

Morphologically, the main body of the pore-throat combination still belongs to the pore, and the only difference between the pore-throat combination and the pure pore is that the former also contains at least one throat. We also took the pore diameter of the

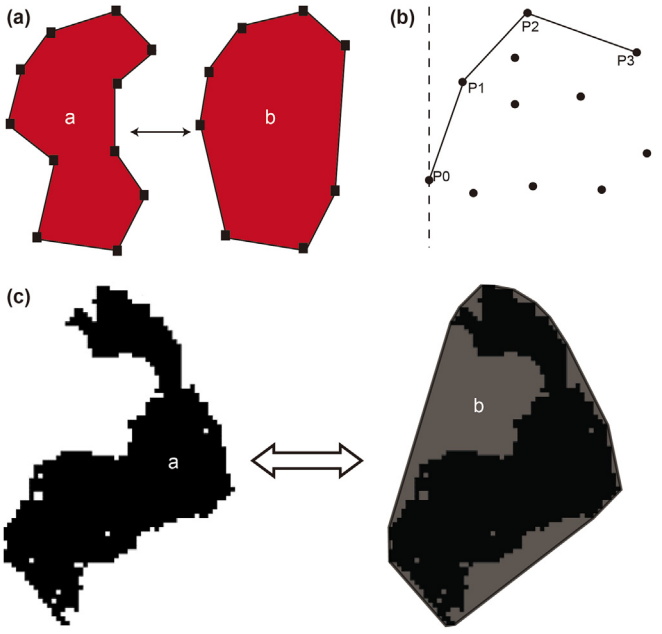

Fig. 3. Schematic diagram of the definition of pore-throat solidity (Note: In Fig. 3(a), "$S_p^{'}$" indicates the area of the pore-throat boundary, and "$S_c^{'}$" indicates the area of the convex hull. Fig. 3(b) indicates the process of convex hull boundary detection. Fig. 3(c) shows "$S_p^{'}$" and "$S_c^{'}$" as obtained in the actual case application.).

pore-throat combination and then incorporated the numerical value into the statistical range of pore parameters.

Given that the transition in the connection between a pore and throat actually acts as the pore, the connection should not be neglected. Therefore, we used the area equivalent radius instead of the radius of the tangential circle to represent the size of the pore. This is an innovation in theory, and the applicability of this method can be verified through comparative results in the next section.

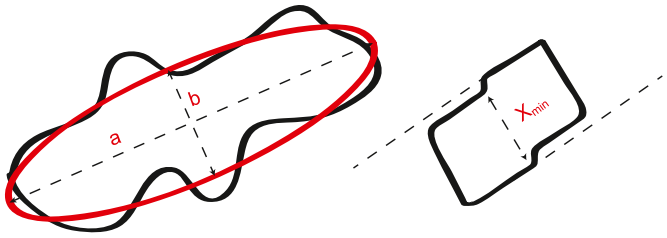

Fig. 5. The Legendre inertial ellipse and minimum Feret diameter. (Note: The Legendre inertia ellipse, marked in red, was fitted by the black pore-throat boundary. The notations "a" and "b" indicate the length of the long and short axes, respectively, of the Legendre inertia ellipse, and X_{min} is the minimum Feret diameter.)

3.3. Image processing aimed at obtaining pore-throat solidity

The current problems with reservoir image processing are mainly the following: (1) a low signal-to-noise ratio, (2) uneven distribution of gray imagery, and (3) uneven imaging of pore and throat boundaries. At present, researchers mainly address the above problems by conducting fine processing of reservoir images, such as denoising (Weickert, 1999), phase boundary enhancement (Pratt, 2001), and region limited phase division (Sheppard et al., 2006). For this study, the mean shift method and bilateral filtering were added to correct the image.

Mean shift is a procedure for locating the maxima of a density function given discrete data sampled from that function, which is

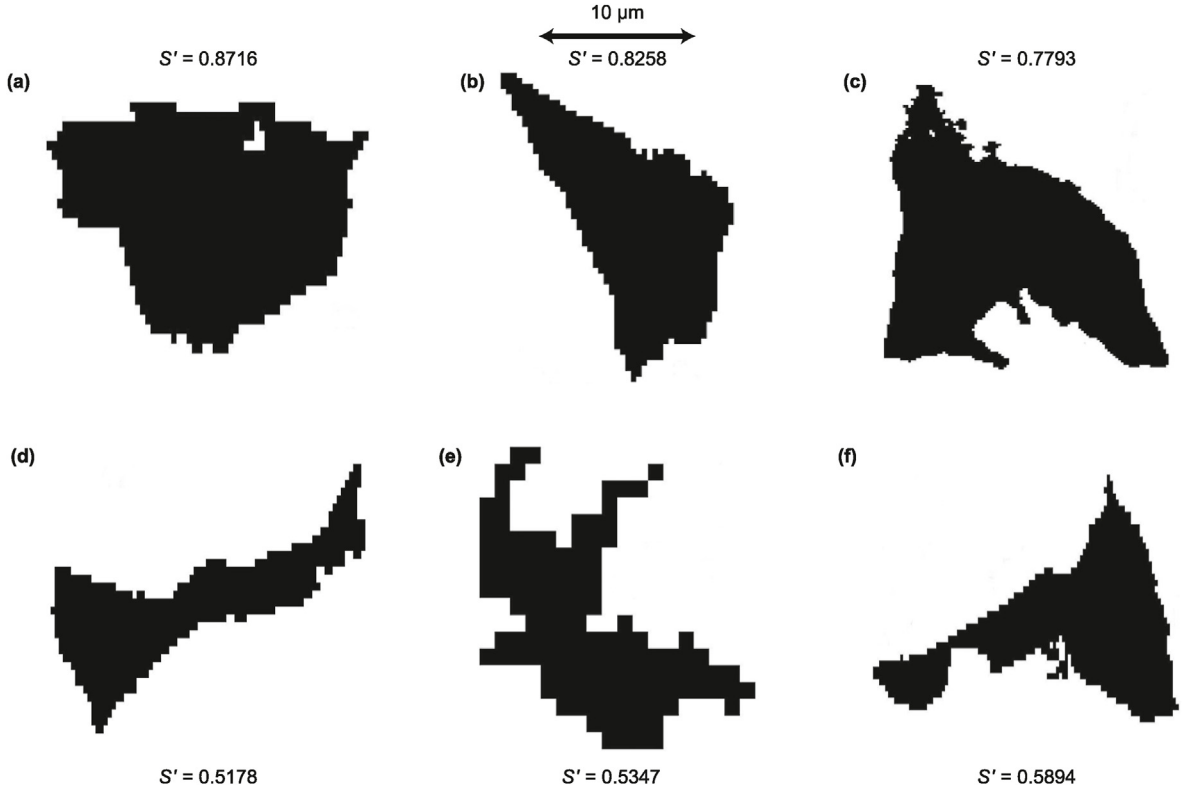

Fig. 4. Pure pores **(a–c)** and pore-throat combinations **(d–f)**. (Note: The $S^{'}$ values for (a–c) are 0.8716, 0.8258, and 0.7793, respectively; the $S^{'}$ values for (d–f) are 0.5178, 0.5347, and 0.5894, respectively.)

useful for detecting shape edges (Ghassabeh and Rudzicz, 2016). Bilateral filtering is a well-known technique for smoothing gray-scale and color images while preserving edges and image details by means of an appropriate nonlinear combination of the color vectors in a neighborhood (Joseph and Periyasamy, 2018). Furthermore, to ensure the accuracy of pore and throat extraction, the planar scan of energy dispersive spectrometer (EDS) analysis was used to identify the fuzzy boundary, which is difficult for the watershed algorithm to accomplish. The mean shift made up for the watershed algorithm's shortcomings when solving the uneven imaging in pore and throat boundaries, ensuring the accuracy of the pore and throat extraction. Given the cost of the planar scan of EDS technology, the accuracy of other models was also checked against our results.

The extraction process of a pore and throat is shown in Fig. 6. First, watershed identification was performed on the original image; the results were then compared with those of EDS to ensure the pores, throats, and particles were distinguished for accurate extraction. The parameters of the pores and throats could then be statistically analyzed.

It is necessary to point out that the FE-SEM resolution was not immutable in this study; it changed with the actual sample size. The actual FE-SEM imaging resolution was 0.48 nm, which allows for the full analysis of the characteristics of nano-sized pores and throats (Zou et al., 2011; Zhu et al., 2016).

Eight samples (sample size: 5 mm × 5 mm, resolution 1 μm) from the Chang 7_2 tight sandstone oil reservoir were used in this study. The high resolution image processing of all samples was first performed, and then the pore-throat solidity of all samples was obtained by Legendre ellipse fitting. The frequency distribution of pore-throat solidity is shown in Fig. 7, and the cumulative probability statistics of all data points were conducted, as evidenced in Fig. 8.

3.4. The concept and identification principle of cutoff point

The cutoff point selection is mainly based on two considerations as presented in Fig. 7. First, the absolute value of the change rate in pore-throat solidity changed (from positive to negative) the demarcation point (i.e., a qualitative change). This coincides with the difference between the pore-throat combination and the pure pore. Pure pore and pore-throat combination are established based on the differences of the geometric parameters. Second, the cumulative probability curve experienced the largest change at the demarcation point, and the increase rate of the cumulative probability has undergone a substantial shift from this point onward.

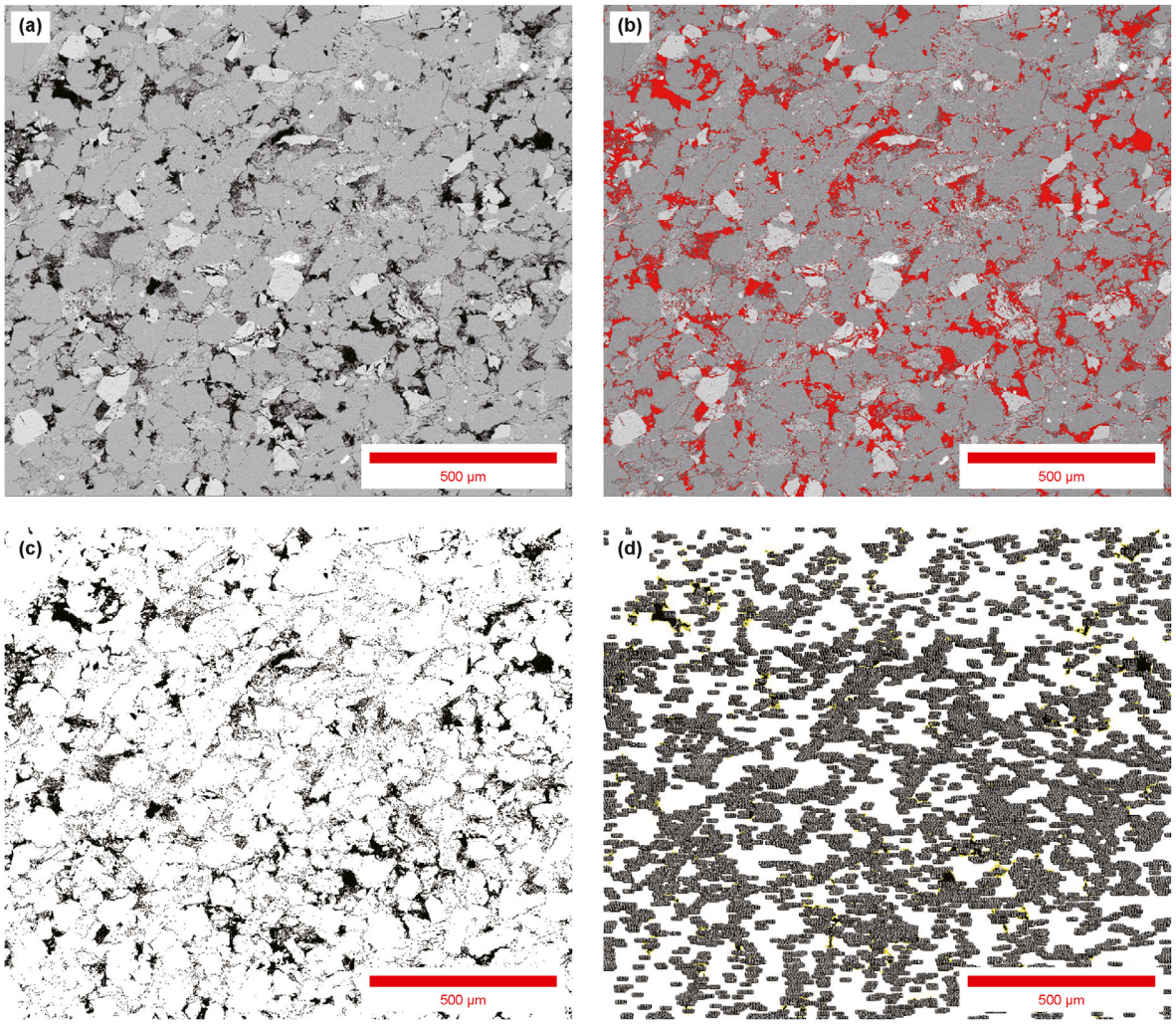

Fig. 6. Image processing of the Chang 7_2 tight sandstone oil reservoir. (Note: The four steps include (**a**) source image acquisition, (**b**) threshold calculation, (**c**) pore-throat extraction, and (**d**) parameters calculation.).

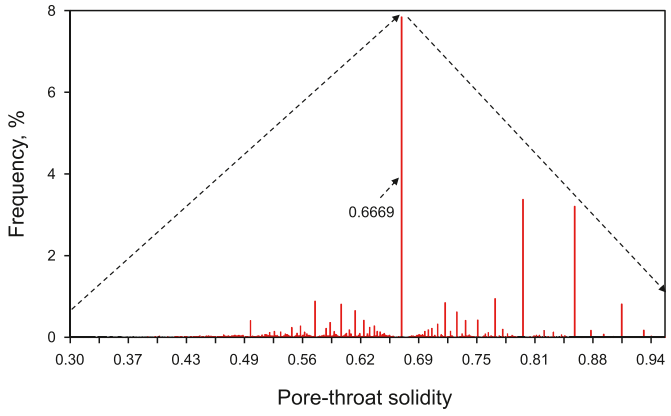

Fig. 7. Frequency distribution for the pore-throat solidity of the Chang 7_2 tight sandstone oil reservoir in the Yanchang Formation, Ordos Basin. (Note: The horizontal axis indicates the pore-throat solidity value, and the vertical axis indicates the frequency of all pore-throat solidity values. The red columns indicate the frequency of individual pores and throats; the value of the highest column is 0.6669. The two black arrows could indicate the frequency trend.)

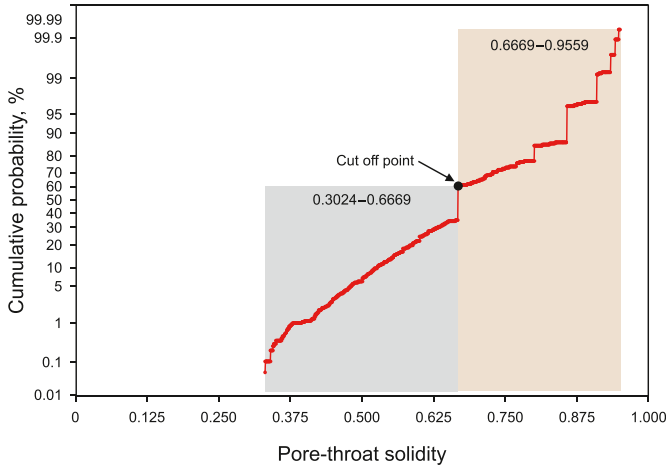

Fig. 8. Cumulative probability distribution curves for the pore-throat solidity of the Chang 7_2 tight sandstone oil reservoir in the Yanchang Formation, Ordos Basin. (Note: The horizontal axis indicates the pore-throat solidity value, and the vertical axis indicates the cumulative probability of all pore-throat solidity values. The red curve indicates the trend of the cumulative distribution of pore-throat solidity. The black point could be identified as the cutoff between the pore-throat combination and the pure pore.)

To further ensure the repeatability and accuracy of the choice of the cutoff point, we selected 10 reservoir samples with various physical properties (i.e., porosity and permeability) from many regions of China, including reservoirs with moderate to high permeability. The new model proposed in this study was used to calculate the pore-throat solidity, and the probability distribution histogram of pore-throat solidity was drawn to determine the cutoff point values.

Therefore, if we want to segment and characterize the pores and throats of an unknown reservoir sample, we must redraw the probability distribution histogram of the pore-throat solidity and recalculate the cutoff point value.

It is necessary to note that in the calculation process, some values of pore-throat solidity could be as much as 1, but we could not use that. It is because the individual whose pore-throat solidity value equals to 1 is only a single pixel, which cannot indicate a complete pore or throat. Thus, the physical meaning of a pore-throat solidity of 1 should be illustrated. The high resolution FE-SEM observations (Fig. 6) show that the actual pure pores are not strictly convex shells (i.e., the pore-throat solidity should be slightly less than or close to 1). Through in-depth observation, we found that the pore and throat bodies with a pore-throat solidity of 1 are the accumulations of 1–3 pixels, which are not the effective pores and throats. Thus, when it came to the actual calculations, these individuals should be removed. Therefore, a pore-throat solidity of 0.6669–0.9559 is defined as a pure pore.

3.5. Other theoretical and technical details

In the image analysis method for pore-throat structures, the individual pores and throats with a diameter less than 3 times that of the pixel diameter were removed. It should be noted that the pretreatment of pore and throat images determined the necessity of this process. Furthermore, the pretreatment results showed that individual pores and throats with a diameter less than 3 times that of the pixel diameter were fitted to the invalid pores and throats (i.e., those with a pore-throat solidity of 1). Therefore, similar processing was performed in this study to ensure the accuracy of the results.

There are many ways to mitigate this deviation to a large extent, such that it does not hinder the logical pore-throat recognition and identification in 2D space. In the practical application of the new model, we tried to reduce this deviation in three ways: (1) cutting multiple slices from different angles and performing high resolution FE-SEM imaging; (2) cutting multiple slices along different positions of the same angle and performing high resolution FE-SEM imaging; and (3) imaging the same slice in different areas and obtaining multiple images. The new model was then applied to identify and segment all these images. Finally, the average value was taken as the final analytical result of a sample. Practical tests show that the deviations caused by the misjudgment of an isolated pore were greatly reduced when following this method.

4. Results

Fig. 4 shows the example of pore network extraction (PNE) after high resolution field emission (FE)-SEM images were taken. It also shows that the pore-throat combination belongs to the generalized concave irregular polygon and that the pore-throat solidity of the pure pore should be generally larger than that of the pore-throat combination. The differences are significant. The smaller the pore-throat solidity, the larger the concavity and the closer it is to the characteristics of the pore-throat combination as opposed to those of the pure pore. Thus, the determination of the cutoff point of the pore-throat solidity value becomes the key to distinguish the pore-throat combination from the pure pore.

We chose to apply our new model and method at Chang 7_2 tight sandstone oil reservoir of the Yanchang Formation, Ordos Basin. Thin sections represented in Fig. 9 show that the dissolved pores and residual inter-grains pores dominate, as do the contractile-neck throats and lamellar curved throats. Limited development of pores and throats leads to low porosity and permeability, and the difference in pore and throat shape is significant, which is helpful to find the automatic identification method.

In general, the cumulative probability distribution curve in Fig. 8 can be divided into two segments: 0.3024–0.6669 and 0.6669–0.9559. Based on the causal link between the particles and the pores and throats, when compared with grain size probability curves, the first obvious inflection point of pore-throat solidity, 0.6669, was defined as the cutoff point between the pore-throat combination and the pure pore. The ranges 0.3024–0.6669 and 0.6669–0.9559 indicate the pore-throat combination and the pure pore, respectively.

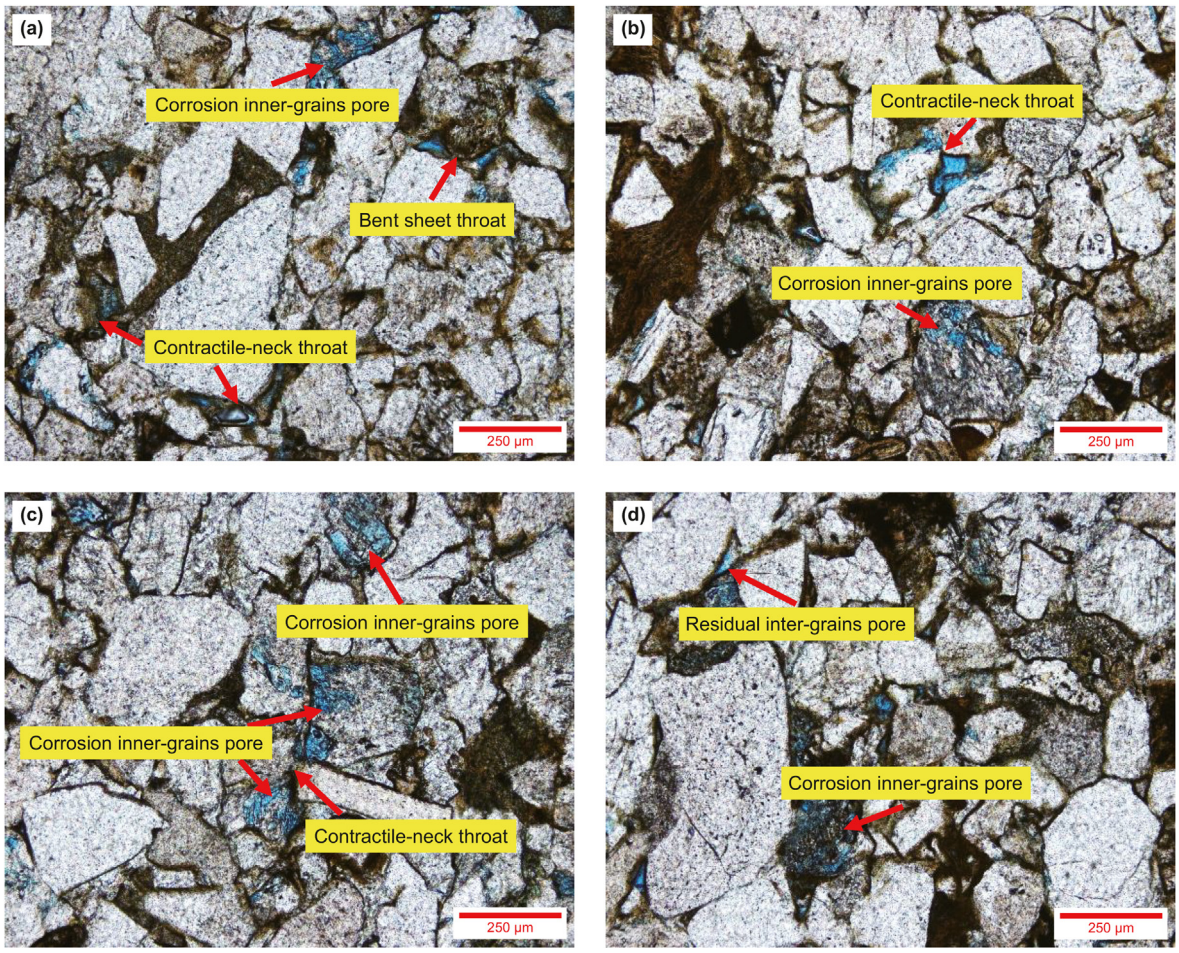

Fig. 9. Thin section observations of the tight sandstone oil reservoir of the Chang 7_2 member of the Yanchang Formation, Ordos Basin. (Note: The blue indicate the pore system; the black characters and red arrows indicate the pore types and locations; the red lines indicate the image scale. Four images **(a, b, c, d)** indicate four samples from four wells, respectively.).

Fig. 10 shows that the cutoff point values have a broad range, which is roughly concentrated between 0.5425 and 0.8060, with an average value of 0.6467. This proves very well that the cutoff point values are not fixed or relatively centralized. This also proves that for reservoir samples of different areas, lithologies, or physical properties, the cutoff point must be different, not all equal to 0.6669, even for different formations in the same area.

By correlating the cutoff point values of 10 samples with the porosity and permeability of each sample (Fig. 11), the cutoff point values demonstrate no obvious relationship in terms of porosity and permeability. Thus, once again, the cutoff point values of pore-throat solidity (i.e., the key point to segments in pore-throat combinations and pure pores) should be determined according to the pore-throat development of specific samples.

The new model was used to calculate the Chang 7_2 tight sandstone oil reservoir samples. The results of the pore-throat identification are shown in Fig. 12.

The statistical results are shown in Fig. 12. The peak pore radius of the Chang 7_2 tight sandstone oil reservoir is 4.89–11.25 μm, and the peak throat radius is 2.03–9.78 μm. We also found that the results will change with the scale and resolution and that comprehensive analysis is still needed.

Values greater than the cutoff point indicate a critical change in pore geometry. It should be noted that the choice of this step and the application effect formed a feedback system of mutual checking, and the actual operation of the trial ultimately determined the best cutoff point. In other words, if we choose the wrong cutoff point value, the calculation results of the new model would be very different from those of the previous model. Thus, we can return to the cutoff point value step and re-select the cutoff point value until we find the best one which enables us to achieve the highest identification accuracy of pure pore and pore-throat combination.

This method of identification has some obvious applications in tight sandstone oil reservoir exploration and development. This method could provide a more accurate understanding of pore-throat identification, Primary work suggests that pores determine reservoir performance and throats determine fluid flow performance (Luo et al., 2022). However, pore-throat identification should serve for the study of fluid filling, exploitation, and reservoir characteristics. Fluid flow is a natural phenomenon and fluids do not flow separately in pores and throats. Therefore, the mechanical separation of all pores and throats is questionable. Furthermore, pores could also play an important role in the fluid flow process. Parts of the throats will also affect the fluid reservoir to a certain extent. Therefore, it is more accurate to identify the pore-throat combinations (not the pure pores) and to calculate the pores and throats on the basis of those combinations (Liu et al., 2021; Xie et al., 2022).

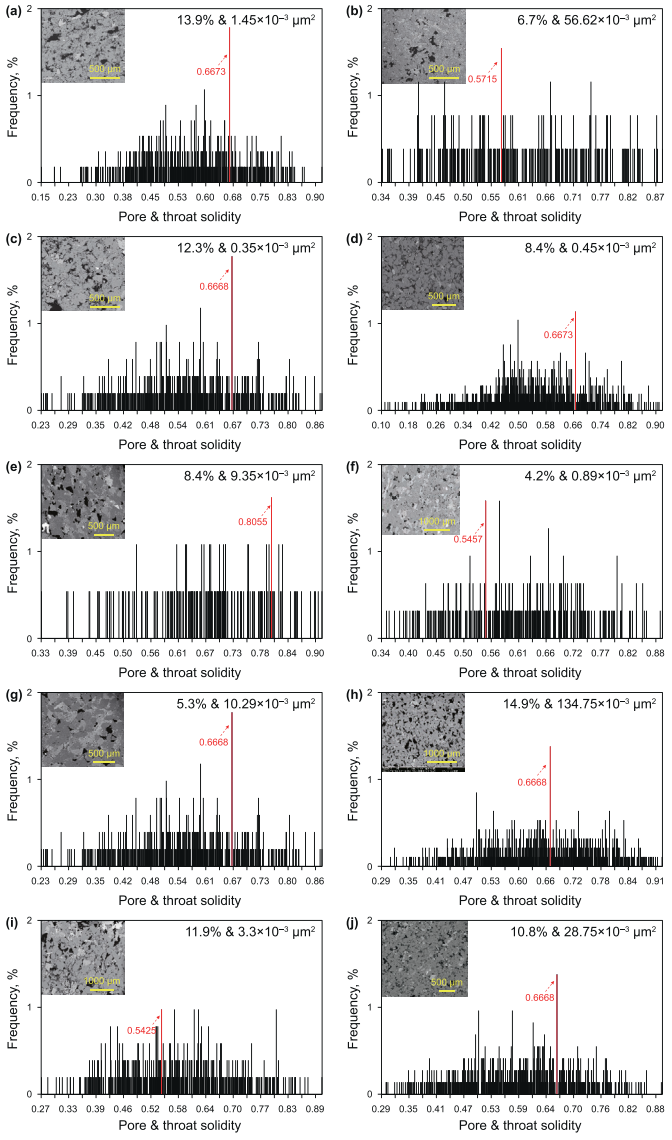

Fig. 10. The pore-throat solidity distribution histogram of multiphysical reservoir samples from different areas of China. (Note: For each plot, the horizontal coordinate of the graph indicates the pore-throat solidity value (dimensionless), and the vertical coordinate of the graph indicates the frequency, %. The red line indicated by the red arrow in the plot corresponds to the cutoff point value determined by this method. The upper left corner of the plot is the corresponding FE-SEM image of the reservoir sample, and the upper right corner is the porosity and then the permeability value of the reservoir sample.).

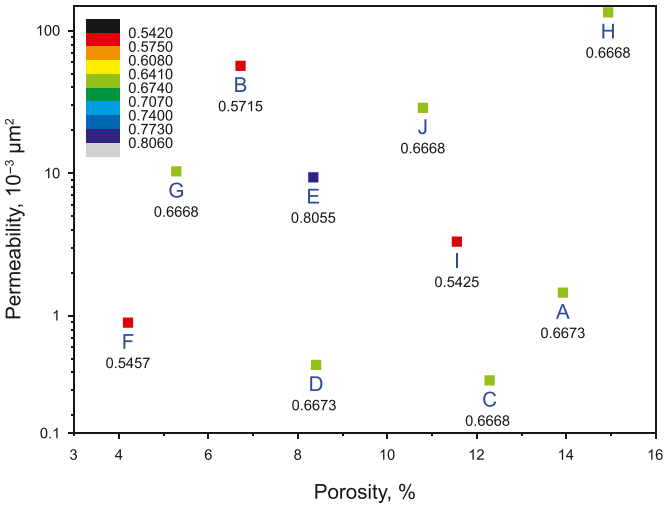

Fig. 11. The relationship between the cutoff point value for the pore-throat solidity value and physical parameters of multiphysical reservoir samples from different areas of China. (Note: Samples A, B and C are low-permeability or tight sandstones from different regions and depths in Songliao Basin, sample D is low-permeability sandstone from Tarim Basin, sample E, F, G and I are low-permeability or tight sandstones from different regions and depths of the Ordos Basin, and sample H is Bailey sandstone. The horizontal axis of the graph indicates the porosity of the samples, the vertical axis indicates their permeability, and the color-coded numerical values indicate their cutoff point values.)

5. Discussions

5.1. Applicability of pore-throat identification in 2D space

The purpose of pore-throat identification and statistical characterization is to clarify the influence of pores and throats on reservoirs and the fluid flow in reservoirs. In 2D space, pores are structures surrounded by skeleton particles (include quartz, potassium feldspar, plagioclase and so on), playing an important role in fluid storage, the relatively narrow parts connecting the pores are the throats. This definition has been widely used and remains the most classical definition of pores and throats (Luo, 1986; Van Eyndhoven et al., 2015; Liu et al., 2015; Putanowicz, 2015; Xiong et al., 2016). We have thus adapted this definition for this study.

Through microscopic observation and simplified model analysis, scholars divided the throats of a clastic rock reservoir into five types: pore-shrinking throats, neck-shrinking throats, sheet throats, curved sheet throats, and tubular bundle throats (Liu et a, 2021; Yin et al., 2021a, 2021b; Xie et al., 2022). Thus, both pores and throats were originally defined in 2D space, and petroleum geologists can use thin sections to study reservoir space development, distinguishing pores and throats through the images of thin sections. Through manual measurement or image processing, rough values of pore and throat size can be obtained.

It should also be noted that these methods are used to segment pore throats in 2D space. Therefore, no problem occurs in pore-throat recognition and identification in 2D space. It should be further noted that some isolated pores we identified on the images in 2D space may be the cross section of throats in three-dimensional (3D) space. It is undeniable that any technology will have deviations, even in 3D space; the key problem should be how to minimize the deviation caused by this probability.

If we accept the recognized definition of a pore or a throat, and if individuals are defined as pores in 3D space, they will also be defined as pores, not throats, in 2D space. The reason is simple: throats are dependent on pores; thus, every throat must have at least two pores. No matter which direction we cut from, pores in 3D space will always be pores in 2D space. Hence, throats that appear in images of 2D space cannot be the cross section of pores in 3D space.

Granted, the introduction of digital core technology has stimulated a shift from 2D to 3D space, leading to numerous innovative findings. However, it does not mean that pores and throats cannot be identified and segmented in 2D space. The classification of pores and throats and the first discovery of nanopores in unconventional reservoirs have both depended largely on microscopic observations in 2D space. Therefore, as digital core technology cannot fundamentally solve two major problems (i.e., high cost and resolution-representativeness conflict), reservoir information on a 2D plane still has great potential for further exploration. The accuracy and practicability of reservoir space characterization also require

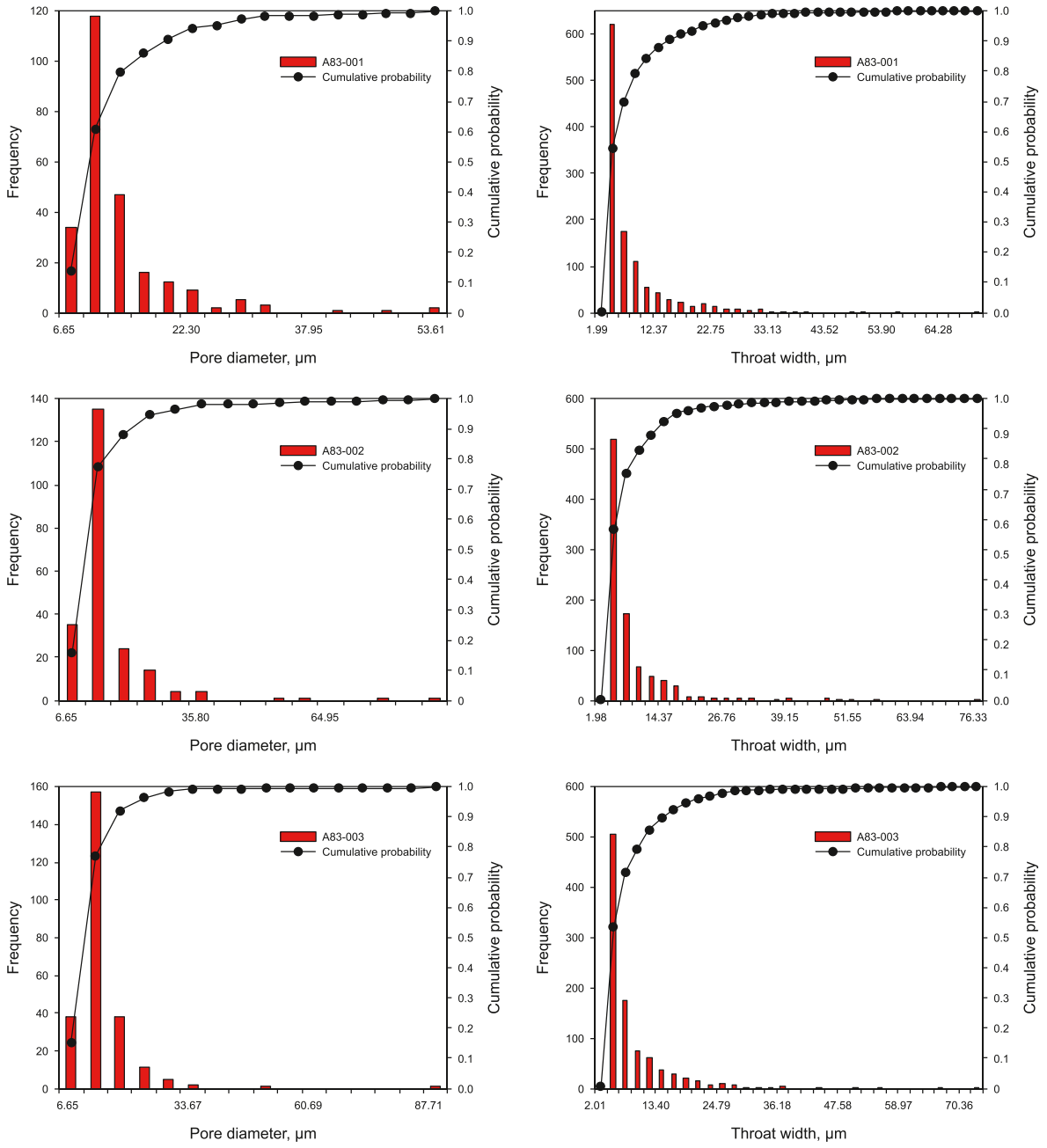

Fig. 12. Pore-throat identification results of the Chang 7_2 tight sandstone oil reservoir in the Yanchang Formation, Ordos Basin. (Note: The red columns indicate the frequency distribution of the pore diameter and throat width. The black lines indicate the cumulative frequency.)

improvements in 2D technology. For unconventional oil and gas reservoirs, it is essential to study the accurate identification and identification model of pores and throats in 2D space.

In addition, the imaging pixels determine the resolution of the image. Higher resolution could help to provide more detailed information and make pores and throats more clearly visible. On the contrary, low resolution images may not accurately display small or densely arranged pores and throats. Given the excellent performance of FE-SEM in two-dimensional space, the best recognition scale for the pores and throats we identified in this study could reach nearly 50 nm, fully meeting the research needs of distinguishing pores and throats in tight sandstone.

5.2. Accuracy evaluation

This study introduces a new model for the identification and statistical analysis of pores and throats in a tight sandstone oil reservoir. The new model applied high resolution FE-SEM, high precision image processing, morphology analysis. Therefore, a comparative analysis of the results from this study and previous research was performed to clarify the nature of the difference and to illustrate the scope of the new method (Tables 1 and 2).

In the existing testing technology, pore-throat identification was primarily conducted using constant-rate mercury injections and micro- or nano-CT. Pore testing technologies have also included nuclear magnetic resonance (NMR) and HPMI. Tables 1 and 2 show the determination data from previous studies of pore and throat

Table 1
Comparison of past and present data on pore radius in the Chang 7 members of the Yanchang Formation.

Literature	Porosity scale, %	Permeability scale, 10^{-3} μm^2	Pore radius scale, μm	Average peak radius of pore, μm	Method
Han et al. (2015)	5–15	0.01–0.5	2–10	5	Micro-CT
Feng et al. (2013)	2.5–12.5	0.009–0.2	0.1–10	8	NMR
Lei et al. (2017)	1.62–10.97	0.001–0.298	1–10	8	NMR
Zhang et al. (2017)	2.5–12	0.031–0.430	0–0.5	0.25	Thin sections
Li, 2016	5–10	0.005–0.25	2–10	5	Micro-CT
Zhong, 2017	5.5–10.3	0.007–0.383	1–100	6.5	HPMI
Zhang et al., 2016	7.6–11.4	0.01–0.38	5–40	17.5	CT
Fan, 2016	4.1–14	0.009–0.302	100–250	170	Constant-rate mercury injection
This study	3.95–12.4	0.006–0.460	3.3–8	7.64	Our method

Table 2
Comparison of past and present data on throat radius in the Chang 7 members of the Yanchang Formation.

Literature	Porosity scale, %	Permeability radius scale, 10^{-3} μm^2	Throat radius scale, μm	Method
Former studies	1.62–15	0.001–0.5	0.08–4	Constant-rate mercury injection, CT
This study	3.95–12.4	0.006–0.460	2–9.78	Our method

radius, respectively.

In Table 1, the results of the physical parameters and pore radius of the tight oil reservoir are listed separately; the methods are also presented.

It should be noted that differences based on different principles are still significant, as evident in Table 1, and the internal mechanism of the differences cannot be ignored. The test results via constant-rate mercury injection (Fan, 2016) differ from those in other studies. The main reason is the difference in the principle of pore size measurement and the calculation mode. Nevertheless, the mechanism should also be clarified.

The advantages of the new model proposed in this study are reflected in two aspects: (1) compared with the existing models, the new model takes the pure pore and pore-throat combination as the basic unit of pore and throat identification, which is more fit to the real geometric characteristics of reservoir spaces; (2) compared with the existing models, the new model considers the physical properties of pore and throat as fluid storage and seepage space completely, the identification of pores and throats can be carried out in a wider scale, which is more conducive to explore and understand the flow behavior of fluid in tight rocks.

Taking the technology of constant-rate mercury injection and CT as an example, the former mainly identifies pores and throats through the pressure fluctuations during mercury injection (He et al., 2011; Yu et al., 2015). When the mercury displacing front passes through a plurality of pores and throats within a short period of time, it inevitably ignores some information (i.e., large pores and small throats). It thus neglects some smaller pressure changes in pores and throats at intermediate intervals because of the sensitivity of the pressure fluctuation amplitude. Consequently, the majority of test results on large pores and small throats are mainly highlighted, and the degree of characterization for the middle range of pores and throats is still worthy of further analysis.

Unlike that of the former method, the analytical principle of CT is mainly based on the difference in diffraction intensity between pore and throat spaces and the mineral matrix. Through the threshold identification algorithm, pores and throats are statistically calculated. In this method, the differences in the pores and throats are thus mainly located in the threshold partition algorithm, identification algorithm, sample size and sample resolution, and its calculation principle is totally different from the constant-pressure mercury test. It also differs from NMR, but the principle and method in this paper fits with CT to a certain degree, so the accuracy is relatively high (Zhang and Zhang, 2021).

As with the analysis of pore radius in Table 1, Table 2 shows the physical parameters and throat radius of the Chang 7_2 tight sandstone compared with other studies. We found that our measurement of physical parameters coincides with that of past research and that the throat analysis results partially overlap with those of past research.

The main reason for the differences in Table 2 is that the calculation principle, sample size, and sample resolution used in this experiment and its theoretical calculations significantly differ from the methods in previous research. Therefore, to prove the applicability of our method and to determine the reasonable use of this method, supplementary experiments were conducted for further verification.

To show that the new model in this paper can fully meet the needs of nanopore and throat characterization in tight sandstone oil reservoirs, we matched the FE-SEM resolution of previous studies (up to 0.48 nm). We also selected two groups of samples with the same sample size (0.5 mm × 0.5 mm) as that of previous studies to conduct the pore-throat identification and statistical analysis in a tight sandstone oil reservoir. These conditions helped to further verify the accuracy of our method (The resolution for Fig. 13 was 3.5 nm/pixel.).

Fig. 13 shows that when we adjusted the sample size and resolution parameters to the values of previous studies, the throat radius of the Chang 7_2 tight sandstone oil reservoir is mainly 80–2000 nm; the average value is 506.3 nm, which has a higher degree of agreement with the conclusions of previous studies in Table 2. Therefore, the peak throat radius of the Chang 7_2 tight sandstone oil reservoir is between 0.08 μm and 9.78 μm, and the multiscale consideration should be further studied. To some extent, our method also reveals that researchers should pay attention to the problem of multiscale fusion in reservoirs as a practical application. The new model proposed in this paper should be applied to different scales to obtain more reasonable results.

Finally, we used synchronous samples to continue the supporting experiments. In CT scanning and SEM imaging of the Chang 7_2 tight sandstone samples, the resolution of the images was consistent. Fig. 14 demonstrates the maximum ball method for SEM imaging used to conduct pore-throat identification statistics, thus verifying the applicability and accuracy of our method.

It should be also pointed out that the sampling layers of the samples involved in Tables 1 and 2 are almost all included in this study, so the results obtained are the distribution range of pores and throats. It is therefore reasonable to compare the data range of

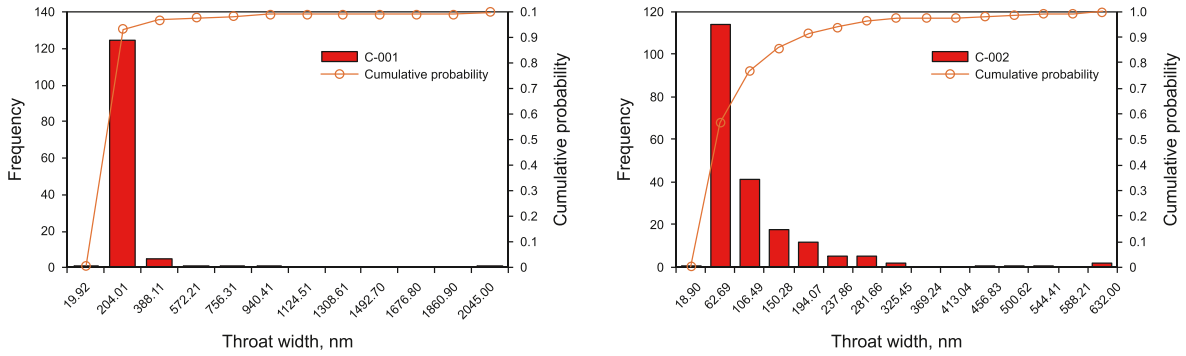

Fig. 13. Throat identification results for the Chang 7_2 tight sandstone oil reservoir samples with high resolution (0.48 nm) at a relatively large scale. (Note: The red columns indicate the frequency distribution of the pore diameter and throat width. The black lines indicate the cumulative frequency.)

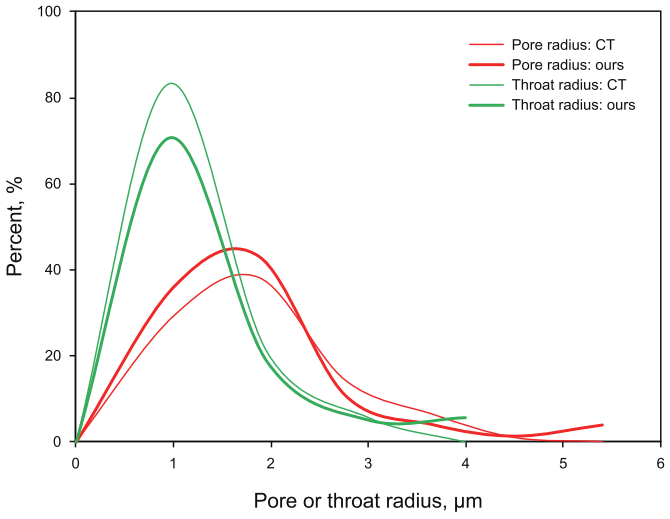

Fig. 14. Comparison of pore-throat identification results for the Chang 7_2 tight sandstone oil reservoir samples under the same sample size and resolution conditions. (Note: The red and green lines indicate the pore and throat radius distributions, respectively. The thick and thin lines indicate the results based on this study's new model and the MB model (CT), respectively.).

pores and throats obtained in this study with them.

We compared analytical results based on CT scanning and the SEM imaging for our model. The experimental results show the overall distribution of pores and throats, and the trend is relatively consistent, precisely reflecting the relative advantage of our new model when finely characterizing small-scaled and large-scaled pore and throat areas. However, as mentioned before, it should be noted that due to the differences in the principle of detection and data analysis, the results for the same reservoir are necessarily different. This also reveals that a variety of test results should be combined in practical applications.

Therefore, only the combination of scale upgrading (upscaling), scale degradation (downscaling) and the complete pore curve construction of the reservoir can fully determine the oil and gas accumulation in a reservoir.

6. Conclusions

The accuracy and practicability of reservoir space characterization depends on improvements in 2D reservoir resolution, the introduction of new characterization parameters, and innovative ideas in reservoir space morphology.

(1) Analogous to the concept particle solidity (used to characterize the geometry of rock particles), we presented a new concept of pore-throat solidity. The cumulative probability of this new parameter can be used to identify two types of individuals in images of a reservoir: the pore-throat combination and the pure pore, thus obtaining the distribution of pores and throats separately.

(2) The advantages of the new model proposed in this study are reflected in two aspects: (a) compared with the existing models, the new model takes the pure pore and pore-throat combination as the basic unit of pore and throat identification, which is more fit to the real geometric characteristics of reservoir spaces; (b) compared with the existing models, the new model considers the physical properties of pore and throat as fluid storage and seepage space completely, the identification of pores and throats can be carried out in a wider scale, which is more conducive to explore and understand the flow behavior of fluid in tight rocks.

(3) This new model pays greater attention to the physical meaning of pores, throats, and the characterization of pore-throat identification. The new model also makes pore-throat identification results more applicable in petroleum research; additionally, it provides a theoretical basis and practical calculation method for the fast and accurate evaluation of tight sandstone reservoirs.

Declaration of competing interest

The authors declare that they have no known competing financial interests or personal relationships that could have appeared to influence the work reported in this paper.

Acknowledgements

This work was jointly supported by Beijing Natural Science Foundation (No. 8232054), Young Elite Scientists Sponsorship Program by CAST (No. YESS20220094), Young Elite Scientists Sponsorship Program by BAST (No. BYESS2023182), Youth Innovation Promotion Association CAS (No. 2023021), and National Natural Science Foundation of China (No. 41902132).

References

Arand, F., Hesser, J., 2017. Accurate and efficient maximal ball algorithm for pore network extraction. Comput. Geosci-UK. 101, 28–37. https://doi.org/10.1016/j.cageo.2017.01.004.

Arzilli, F., Cilona, A., Mancini, L., Tondi, E., 2016. Using synchrotron X-ray microtomography to characterize the pore network of reservoir rocks: a case study on carbonates. Adv. Water Resour. 95, 254–263. https://doi.org/10.1016/j.advwatres.2015.07.016.

Bai, B., Zhu, R.K., Wu, S.T., Cui, J.W., Su, L., Li, T.T., 2014. New micro-throat structural characterization techniques for unconventional tight hydrocarbon reservoir. China Petroleum Exploration 19 (3), 78. https://doi.org/10.3969/j.issn.1672-7703.2014.03.010.

Berrezueta, E., Kovacs, T., 2017. Application of optical image analysis to the assessment of pore space evolution after CO_2 injection in sandstones. A case study. J. Petrol. Sci. Eng. 159, 679–690. https://doi.org/10.1016/j.petrol.2017.08.039.

Cai, L.X., Xiao, G.L., Lu, S.F., Wang, J., Wu, Z.Q., 2019. Spatial-temporal coupling between high-quality source rocks and reservoirs for tight sandstone oil and gas accumulations in the Songliao Basin, China. Int. J. Min. Sci. Technol. 29 (3), 387–397. https://doi.org/10.1016/j.ijmst.2019.03.006.

Cao, B., Sun, W., Li, J., 2021. Reservoir petrofacies—a tool for characterization of reservoir quality and pore structures in a tight sandstone reservoir: a study from the sixth member of Upper Triassic Yanchang Formation, Ordos Basin. China. J. Petrol. Sci. Eng. 199, 108294. https://doi.org/10.1016/j.petrol.2020.108294.

Cormen, T.H., Leiserson, C.E., Rivest, R.L., Stein, C., 2001. Finding the Convex Hull. Introduction to Algorithms, pp. 947–957.

Darby, B.J., Ritts, B.D., 2002. Mesozoic contractional deformation in the middle of the Asian tectonic collage: the intraplate Western Ordos fold-thrust belt, China. Earth Planet Sci. Lett. 205 (1–2), 13–24. https://doi.org/10.1016/S0012-821X(02)01026-9.

Dong, H., 2008. Micro-CT Imaging and Pore Network Extraction. Doctoral dissertation, Department of Earth Science and Engineering. Imperial College London.

Du, S.H., Pang, S., Shi, Y.M., 2018a. A new and more precise experiment method for characterizing the mineralogical heterogeneity of unconventional hydrocarbon reservoirs. Fuel 232, 666–671. https://doi.org/10.1016/j.fuel.2018.06.012.

Du, S.H., Pang, S., Shi, Y.M., 2018b. Quantitative characterization on the microscopic pore heterogeneity of tight oil sandstone reservoir by considering both the resolution and representativeness. J. Petrol. Sci. Eng. 169, 388–392. https://doi.org/10.1016/j.petrol.2018.05.058.

Du, S.H., Shi, G.X., Yue, X.J., Kou, G., Zhou, B., Shi, Y.M., 2019. Imaging-based characterization of perthite in the Upper Triassic Yanchang formation tight sandstone of the Ordos Basin, China. Acta Geologica Sinica-English Edition 93 (2), 373–385.

Fan, M.M., 2016. Study on Chang-7 Tight Reservoir Characteristics of Triassic Yanchang Formation in Ordos Basin. Northwest University.

Faria, N., Pons, M.N., De Azevedo, S.F., Rocha, F.A., Vivier, H., 2003. Quantification of the morphology of sucrose crystals by image analysis. Powder Technol. 133 (1–3), 54–67. https://doi.org/10.1016/S0032-5910(03)00078-0.

Feng, S.B., Niu, X.B., Liu, F., Yang, X., Liu, X.J., You, Y., Wang, F., 2013. Characteristics of Chang7 tight oil reservoir space in Ordos basin and its significance. J. Cent. S. Univ. 44 (11), 4574–4580.

Gan, H.J., Xiao, X.M., Lu, Y.C., Jin, Y.B., Tian, H., Liu, D.H., 2007. Genetic relationship between natural gas dispersal zone and uranium accumulation in the Northern Ordos Basin, China. Acta. Geol. Sin-Engl. 81 (3), 501–509. https://doi.org/10.1111/j.1755-6724.2007.tb00973.x.

Ghassabeh, Y.A., Rudzicz, F., 2016. The mean shift algorithm and its relation to kernel regression. Inf. Sci. 348, 198–208. https://doi.org/10.1016/j.ins.2016.02.020.

Gong, X.M., Teng, Q.Z., Wang, Z.Y., Xu, Y.J., 2016. Throat Identification of 3D Rock Image Based on Skeleton. Journal Of Sichuan University, Engineering Science Edition, pp. 100–106. https://doi.org/10.15961/j.jsuese.2016.s2.016.

Gundogar, A.S., Ross, C.M., Akin, S., Kovscek, A.R., 2016. Multiscale pore structure characterization of Middle East carbonates. J. Petrol. Sci. Eng. 146, 570–583. https://doi.org/10.1016/j.petrol.2016.07.018.

Guo, Y.R., Liu, J.B., Yang, H., Liu, Z., Fu, J.H., Yao, J.L., Xu, W.L., Zhang, Y.L., 2012. Hydrocarbon accumulation mechanism of low permeable tight lithologic oil fields in the Yanchang Formation, Ordos Basin, China. Petroleum Exploration and Development Online 39 (4), 447–456. https://doi.org/10.1016/S1876-3804(12)60061-5.

Han, W.X., Gao, C.H., Han, X., 2015. Application of NMR and micrometer and nanometer CT technology in research of tight reservoir: Taking Chang 7 Member in Ordos Basin as an example. Fault-Block Oil Gas Field 22 (1), 62–66. https://doi.org/10.6056/dkyqt201501013.

He, S.L., Jiao, C.Y., Wang, J.G., Luo, F.P., Zou, L., 2011. Discussion on the differences between constant-speed mercury injection and conventional mercury injection techniques. Duankuai Youqitian 18 (2), 235–237.

Jarvis, R.A., 1973. On the identification of the convex hull of a finite set of points in the plane. Inf. Process. Lett. 2 (1), 18–21. https://doi.org/10.1016/0020-0190(73)90020-3.

Jia, C.Z., Zheng, M., Zhang, Y.F., 2014. Four important theoretical issues of unconventional petroleum geology. Acta Pet. Sin. 35 (1), 1. https://doi.org/10.7623/syxb201401001.

Jiang, M.L., Zhang, Y.F., Liu, Y., 2021. Analyzing the micro-pore characteristics of tight oil reservoirs through the implementation of mercury intrusion technique. Arabian J. Geosci. 14 (17), 1787. https://doi.org/10.1007/s12517-021-08055-6.

Jin, Z.J., Zhang, J.C., Tang, X., 2022. Unconventional natural gas accumulation system. Nat. Gas. Ind. B 9 (1), 9–19. https://doi.org/10.1016/j.ngib.2021.08.013.

Jiu, B., Huang, W.H., Li, Y., He, M.Q., 2021. Influence of clay minerals and cementation on pore throat of tight sandstone gas reservoir in the eastern Ordos Basin, China. J. Nat. Gas Sci. Eng. 87, 103762. https://doi.org/10.1016/j.jngse.2020.103762.

Joseph, J., Periyasamy, R., 2018. An image driven bilateral filter with adaptive range and spatial parameters for denoising magnetic resonance images. Comput. Electr. Eng. 69, 782–795. https://doi.org/10.1016/j.compeleceng.2018.02.033.

Kong, X.X., Xiao, D.S., Jiang, S., Lu, S.F., Sun, B., Wang, J.M., 2020. Application of the combination of high-pressure mercury injection and nuclear magnetic resonance to the classification and evaluation of tight sandstone reservoirs: a case study of the Linxing Block in the Ordos Basin. Nat. Gas. Ind. B 7 (5), 433–442. https://doi.org/10.1016/j.ngib.2020.09.001.

Lai, J., Wang, G.W., 2015. Fractal analysis of tight gas sandstones using high-pressure mercury intrusion techniques. J. Nat. Gas Sci. Eng. 24, 185–196. https://doi.org/10.1016/j.jngse.2015.03.027.

Lai, J., Wang, G.W., Fan, Z., Chen, Y.J., Wang, S.C., Zhou, Z.L., Fan, X.Q., 2016. Insight into the pore structure of tight sandstones using NMR and HPMI measurements. Energy Fuels 30 (12), 10200–10214. https://doi.org/10.1021/acs.energyfuels.6b01982.

Lai, J., Wang, G.W., Fan, Z.Y., Zhou, Z.L., Chen, J., Wang, S.C., 2018a. Fractal analysis of tight shaly sandstones using nuclear magnetic resonance measurements. AAPG Bull. 102 (2), 175–193. https://doi.org/10.1306/0425171609817007.

Lai, J., Wang, G.W., Wang, Z.Y., Chen, J., Pang, X.J., Wang, S.C., Zhou, Z.L., He, Z.B., Qin, Z.Q., Fan, X.Q., 2018b. A review on pore structure characterization in tight sandstones. Earth Sci. Rev. 177, 436–457. https://doi.org/10.1016/j.earscirev.2017.12.003.

Lei, Q.H., Cheng, L.B., Wang, C., Fan, J.M., He, Y.A., Zhao, G.X., 2017. A study on distribution features of movable fluids for Chang 7 tight reservoir in Ordos Basin. Nat. Gas Geosci. 28 (1). https://doi.org/10.11764/j.issn.1672-1926.2016.11.017.

Li, Q.D., 2016. Researching on Characteristics of Chang-7 Tight Oil Reservoir in An-83 Area. Northwest University, Xin'an'bian Oilfield.

Li, X.B., Chen, Q.L., Liu, H.Q., Wan, Y.R., Wei, L.H., Liao, J.B., Long, L.W., 2011. Features of sandy debris flows of the Yanchang Formation in the Ordos Basin and its oil and gas exploration significance. Acta Geol. Sin-Engl. 85 (5), 1187–1202. https://doi.org/10.1111/j.1755-6724.2011.00250.x.

Li, Y., Chi, Y.N., Han, S.L., Miao, Y.N., Chen, L., 2021a. Investigation on CT characterization of pore structure in nylon-uncured rubber composite from a microscopic view. Sci. Rep-UK. 11 (1), 15682. https://doi.org/10.1038/s41598-021-95178-1.

Liu, G.F., Zhang, T.H., Xie, Q.C., Liu, W.T., Wang, L.H., Yang, D.Y., 2021. Experimental evaluation of live oil oxidation together with its physical properties during air injection in a tight oil reservoir. Fuel 283, 119121. https://doi.org/10.1016/j.fuel.2020.119121.

Li, Y., Chi, Y.M., Han, S.L., Zhao, C.J., Miao, Y.N., 2021b. Pore-throat structure characterization of carbon fiber reinforced resin matrix composites: Employing Micro-CT and Avizo technique. PLoS One 16 (9), e0257640. https://doi.org/10.1371/journal.pone.0257640.

Liu, H.F., Ma, C.H., Zhu, C.Q., 2022. X-ray micro CT based characterization of pore-throat network for marine carbonates from South China Sea. Appl. Sci. 12 (5), 2611. https://doi.org/10.3390/app12052611.

Liu, X.J., Xiong, J., Liang, L.X., 2015. Investigation of pore structure and fractal characteristics of organic-rich Yanchang formation shale in central China by nitrogen adsorption/desorption analysis. J. Nat. Gas Sci. Eng. 22, 62–72. https://doi.org/10.1016/j.jngse.2014.11.020.

Liu, Y.C., Teng, Q.Z., He, X.H., Yang, X.M., 2012. Improved Throat Finding Algorithm of 3D Core Images. Journal of Sichuan University, Engineering Science Edition, pp. 171–176. https://doi.org/10.15961/j.jsuese.2012.s1.013.

Luo, X.P., Zhang, Y.B., Zhou, H.P., He, K.Z., Zhang, B.Y., Zhang, D.M., Xiao, W.J., 2022. Pore structure characterization and seepage analysis of ionic rare earth orebodies based on computed tomography images. Int. J. Min. Sci. Technol. 32 (2), 411–421. https://doi.org/10.1016/j.ijmst.2022.02.006.

Luo, Z.T., 1986. Pore Structure of Oil and Gas Reservoirs. Science Press, Beijing.

Lyu, Q.F., Wu, H., Li, X., 2021b. A 3D model reflecting the dynamic generating process of pore networks for geological porous media. Comput. Geotech. 140, 104444. https://doi.org/10.1016/j.compgeo.2021.104444.

Mikli, V., Kaerdi, H., Kulu, P., Besterci, M., 2001. Characterization of powder particle morphology. Proc. Est. Acad. Sci.: Engineering(Estonia). 7 (1), 22–34.

Pirard, E., 2004. Image measurements. In: Francus, P. (Ed.), Image Analysis, Sediments and Paleo-Environments. Kluwer academic publishers, Dordrecht, The Netherlands (Chapter 4).

Pratt, W.K., 2001. Digital Image Processing. Wiley Inter-science, California.

Putanowicz, R., 2015. Implementation of pore microstructure model generator and pore space analysis tools. Procedia Eng. 108, 355–362. https://doi.org/10.1016/j.proeng.2015.06.158.

Rabbani, A., Jamshidi, S., Salehi, S., 2014. An automated simple algorithm for realstic pore network extraction from micro-tomography images. J. Petrol. Sci. Eng. 123, 164–171. https://doi.org/10.1016/j.petrol.2014.08.020.

Russ, J.C., 1998. The Image Processing Handbook. CRC Press, Boca Raton, Florida.

Sharqawy, M.H., 2016. Construction of pore network models for Berea and Fontainebleau sandstones using non-linear programing and optimization techniques. Adv. Water Resour. 98, 198–210. https://doi.org/10.1016/j.advwatres.2016.10.023.

Sheng, G.L., Su, Y.L., Zhao, H., Liu, J.H., 2020. A unified apparent porosity/permeability model of organic porous media: coupling complex pore structure and multimigration mechanism. Advances in Geo-Energy Research 4 (2), 115–125. https://doi.org/10.26804/ager.2020.02.01.

Sheppard, A.P., Arns, C.H., Sakellariou, A., Senden, T.J., Sok, R.M., Averdunk, H., Limaye, A., Knackstedt, M.A., 2006. Quantitative properties of complex porous materials calculated from x-ray μCT images. In: Developments in X-Ray Tomography 6318, pp. 326–340. https://doi.org/10.1117/12.679205. SPIE.

Silin, D.B., Jin, G., Patzek, T.W., 2003. Robust determination of the pore space morphology in sedimentary rocks. In: SPE Annual Technical Conference and Exhibition, SPE-84296.
Smal, P., Gouze, P., Rodriguez, O., 2018. An automatic segmentation algorithm for retrieving sub-resolution porosity from X-ray tomography images. J. Petrol. Sci. Eng. 166, 198–207. https://doi.org/10.1016/j.petrol.2018.02.062.
Van Eyndhoven, G., Kurttepeli, M., Van Oers, C.J., Cool, P., Bals, S., Batenburg, K.J., Sijbers, J., 2015. Pore reconstruction and segmentation (PORES) method for improved porosity quantification of nanoporous materials. Ultramicroscopy 148, 10–19. https://doi.org/10.1016/j.ultramic.2014.08.008.
Visher, G.S., 1969. Grain size distributions and depositional processes. J. Sediment. Res. 39 (3). https://doi.org/10.1029/94PA03355.
Walton, W., 1948. Feret's statistical diameter as a measure of particle size. Nature 162, 329–330. https://doi.org/10.1038/162329b0.
Wang, M., Huang, K., Xie, W.D., Dai, X.G., 2019. Current research into the use of supercritical CO_2 technology in shale gas exploitation. Int. J. Min. Sci. Technol. 29 (5), 739–744. https://doi.org/10.1016/j.ijmst.2018.05.017.
Wang, X.Z., Zhang, L.X., Gao, C., 2015. The heterogeneity of lacustrine shale gas reservoir in Yanchang Formation, Xiasiwan area, Ordos Basin. Acta Geol. Sin-Engl. 89 (s1), 99–101. https://doi.org/10.1111/1755-6724.12302_42.
Wang, Z., Tang, H.M., Yang, J., Huang, L., 2022. Reservoir pore characteristics based on depositional microfacies control in the Neogene Guantao formation, Bohai Bay basin, China. Energies 15 (8), 2870. https://doi.org/10.3390/en15082870.
Weickert, J., 1999. Coherence-enhancing diffusion filtering. Int. J. Comput. Vis. 31, 111–127.
Wood, D.A., 2021. Techniques used to calculate shale fractal dimensions involve uncertainties and imprecisions that require more careful consideration. Advances In Geo-Energy Research 5 (2), 153–165. https://doi.org/10.46690/ager.2021.02.05.
Xie, L.L., You, Q., Wang, E.Z., Li, T., Song, Y.C., 2022. Quantitative characterization of pore size and structural features in ultra-low permeability reservoirs based on X-ray computed tomography. J. Petrol. Sci. Eng. 208, 109733. https://doi.org/10.1016/j.petrol.2021.109733.
Xiong, F.Y., Jiang, Z.X., Amooie, M.A., Soltanian, M.R., Moortgat, J., 2017. Pore structure of transitional shales in the Ordos Basin, NW China: Effects of composition on gas storage capacity. Fuel 206, 504–515. https://doi.org/10.1130/abs/2017NE-291062.
Xiong, F.Y., Jiang, Z.X., Chen, J.F., Wang, X.Z., Huang, Z.L., Liu, G.H., Chen, F.R., Li, Y.R., Chen, L., Zhang, L.X., 2016. The role of the residual bitumen in the gas storage capacity of mature lacustrine shale: a case study of the Triassic Yanchang shale, Ordos Basin, China. Mar. Petrol. Geol. 69, 205–215. https://doi.org/10.1016/j.marpetgeo.2015.10.022.
Xu, Y.Q., Liu, L.Y., Zhu, Y.S., 2021. Characteristics of movable fluids in tight sandstone reservoir and its influencing factors: a case study of Chang 7 reservoir in the Southwestern of Ordos Basin. J. Pet. Explor. Prod. Technol. 11, 3493–3507. https://doi.org/10.1007/s13202-021-01250-x.
Yang, H., Deng, X.Q., 2013. Deposition of Yanchang Formation deep-water sandstone under the control of tectonic events in the Ordos Basin. Petrol. Explor. Dev. 40 (5), 549–557. https://doi.org/10.1016/S1876-3804(13)60072-5.
Yang, W.Z., Hou, J.G., Liu, Y.M., Dou, L.X., Wang, X.X., 2022. The pore structures of different lithofacies in low-permeability sandy conglomerate reservoirs and their diagenetic impacts: a case study from the Es4 member of the northern steep slope in Dongying depression, Bohai Bay Basin, NE China. Mar. Petrol. Geol. 136, 105481. https://doi.org/10.1016/j.marpetgeo.2021.105481.
Yang, Z.F., Tang, Y., Guo, X.G., Huang, L.L., Chang, Q.S., 2021. Diagenesis and reservoir space types of alkaline lake-type shale in Fengcheng formation of Mahu Sag, Junggar basin, China. Arabian J. Geosci. 14 (22), 2356. https://doi.org/10.1007/s12517-021-08634-7.
Yao, J.L., Zhao, Y.D., Liu, G.L., Qi, Y.L., Li, Y.H., Luo, A.X., Zhang, X.L., 2018. Formation patterns of Chang 9 oil reservoir in Triassic Yanchang Formation, Ordos Basin, NW China. Petrol. Explor. Dev. 45 (3), 389–401. https://doi.org/10.1016/S1876-3804(18)30044-2.
Yin, D.Y., Wang, D.Q., Zhou, Y.Z., Zhang, C.L., 2021b. Pore structure characteristics of ultra-Low permeability reservoirs. Nat. Resour. Res. 30, 451–462. https://doi.org/10.1007/s11053-020-09709-0.
Yin, S.H., Chen, X., Yan, R.F., Wang, L.M., 2021a. Pore structure characterization of undisturbed weathered crust elution-deposited rare earth ore based on X-ray micro-CT scanning. Minerals 11 (3), 236. https://doi.org/10.3390/min11030236.
Yu, J., Ma, J., Lu, J.G., Cao, Y., Feng, S.B., Li, W.C., 2015. Application of mercury injection and rate-controlled mercury penetration in quantitative characterization of microscopic pore structure of tight reservoirs: a case study of the Chang7 reservoir in Huachi-Heshui area, the Ordos Basin. Petroleum Geology and Experiment 37 (6), 789–795. https://doi.org/10.11781/sysydz201506789.
Zeng, Y.J., Du, S.H., Zhang, X., Zhang, B.P., Liu, H.L., 2020. The crucial geometric distinctions of microfractures as the indispensable transportation channels in hydrocarbon-rich shale reservoir. Energy Rep. 6, 2056–2065. https://doi.org/10.1016/j.egyr.2020.07.004.
Zhang, B.Y., He, Q.Y., Lin, Z.B., Li, Z.H., 2021. Experimental study on the flow behaviour of water-sand mixtures in fractured rock specimens. Int. J. Min. Sci. Technol. 31 (3), 377–385. https://doi.org/10.1016/j.ijmst.2020.09.001.
Zhang, F., Zhang, C., 2021. Evaluating the potential of carbonate sub-facies classification using NMR longitudinal over transverse relaxation time ratio. Advances in Geo-Energy Research 5 (1), 87–103. https://doi.org/10.46690/ager.2021.01.09.
Zhang, H., Chen, G., Zhu, Y.S., Dang, Y.C., Chen, J., Wang, H.L., Si, Y., Bai, C., Li, X., 2017. Quantitative characterization of microscopic Pore & Throat structure in tight sandstone oil reservoirs: a case study of Chang7 reservoir in Xin' anbian oil field, Ordos Basin. Petroleum Geology and Experiment 39 (1), 112–119. https://doi.org/10.11781/sysydz201701112.
Zhang, L.H., Liu, X.Y., Zhao, Y.L., Zhou, Y., Shan, B.C., 2020. Effect of pore throat structure on micro-scale seepage characteristics of tight gas reservoirs. Nat. Gas. Ind. B 7 (2), 160–167. https://doi.org/10.1016/j.ngib.2020.03.002.
Zhang, Z.Y., Chen, S.J., Yao, J.L., Liu, X., Zhao, Y.Q., 2016. A study on microscopic pore characteristics of tight reservoir of Chang 7 sedimentation section of Yanchang Formation, Ordos Basin. Journal of Southwest Petroleum University (Science & Technology Edition) 38 (6), 70. https://doi.org/10.11885/j.issn.1674-5086.2015.05.01.02.
Zhong, D.K., 2017. Micro-petrology, pore throat characteristics and genetic mechanism of tight oil reservoirs—a case from the 6th and 7th members of Triassic Yanchang Formation in Ordos Basin. Oil Gas Geol. 38 (1), 49–61. https://doi.org/10.11743/ogg20170106.
Zhou, S.D., Liu, D.M., Cai, Y.D., Yao, Y.B., Li, Z.T., 2017. 3D characterization and quantitative evaluation of pore-fracture networks of two Chinese coals using FIB-SEM tomography. Int. J. Coal Geol. 174, 41–54. https://doi.org/10.1016/j.coal.2017.03.008.
Zhu, R.K., Wu, S.T., Su, L., Cui, J.W., Mao, Z.G., Zhang, X.X., 2016. Problems and future works of porous texture characterization of tight reservoirs in China. Acta Pet. Sin. 37 (11), 1323. https://doi.org/10.7623/syxb201611001.
Zou, C.N., Zhai, G.M., Zhang, G.Y., Wang, H.J., Zhang, G.S., Li, J.Z., Wang, Z.M., Wen, Z.X., Ma, F., Liang, Y.B., Yang, Z., Li, X., Liang, K., 2015. Formation, distribution, potential and prediction of global conventional and unconventional hydrocarbon resources. Petrol. Explor. Dev. 42 (1), 14–28. https://doi.org/10.1016/S1876-3804(15)60002-7.
Zou, C.N., Zhu, R.K., Bai, B., Yang, Z., Wu, S.T., Su, L., Dong, D.Z., Li, X.J., 2011. First discovery of nano-pore throat in oil and gas reservoir in China and its scientific value. Acta Petrol. Sin. 27 (6), 1857–1864.